Biosensors and Bioelectronics 74 (2015) 37–44

Contents lists available at ScienceDirect

Biosensors and Bioelectronics

journal homepage: www.elsevier.com/locate/bios

A self-referencing biosensor for real-time monitoring of physiological ATP transport in plant systems

Diana C. Vanegas [a,b], Greg Clark [c], Ashley E. Cannon [c], Stanley Roux [c], Prachee Chaturvedi [d], Eric S. McLamore [a,*]

[a] Agricultural and Biological Engineering Department, University of Florida, Gainesville, USA
[b] Food Engineering Department, Universidad del Valle, Cali, Colombia
[c] Department of Molecular Biosciences, University of Texas, Austin, USA
[d] Department of Mechanical Engineering, University of Colorado, Denver, USA

ARTICLE INFO

Article history:
Received 1 April 2015
Received in revised form
9 May 2015
Accepted 9 May 2015
Available online 29 May 2015

Keywords:
Self-referencing
Biosensor
ATP
Graphene
Nanoplatinum
Plant physiology

ABSTRACT

The objective of this study was to develop a self-referencing electrochemical biosensor for the direct measurement of ATP flux into the extracellular matrix by living cells/organisms. The working mechanism of the developed biosensor is based on the activity of glycerol kinase and glycerol-3-phosphate oxidase. A stratified bi-enzyme nanocomposite was created using a protein-templated silica sol gel encapsulation technique on top of graphene-modified platinum electrodes. The biosensor exhibited excellent electrochemical performance with a sensitivity of 2.4 ± 1.8 nA/μM, a response time of 20 ± 13 s and a lower detection limit of 1.3 ± 0.7 nM. The self-referencing biosensor was used to measure exogenous ATP efflux by (i) germinating *Ceratopteris* spores and (ii) growing *Zea mays* L. roots. This manuscript demonstrates the first development of a non-invasive ATP micro-biosensor for the direct measurement of eATP transport in living tissues. Before this work, assays of eATP have not been able to record the temporally transient movement of ATP at physiological levels (nM and sub-nM). The method demonstrated here accurately measured [eATP] flux in the immediate vicinity of plant cells. Although these proof of concept experiments focus on plant tissues, the technique developed herein is applicable to any living tissue, where nanomolar concentrations of ATP play a critical role in signaling and development. This tool will be invaluable for conducting hypothesis-driven life science research aimed at understanding the role of ATP in the extracellular environment.

1. Introduction

Adenosine-5′-triphosphate (ATP) is a multi-functional molecule that is the cornerstone of cell biology. Inside cells, ATP mediates biological reactions involving energy metabolism, cell signaling, cell structure, locomotion, and synthesis of macromolecules (including DNA and RNA). Outside of cells, extracellular ATP (eATP) is a hormone-like signal that regulates diverse physiological responses in animal and plant cells (Burnstock, 2012; Clark et al., 2014). Over the last few years, several approaches have been developed for measuring eATP *in vivo*. The preferred method for measuring eATP has been the luciferase assays, which has been used to document release of ATP from animal cells (Zhang et al., 2008), plant cells (Kim et al., 2006; Clark et al., 2011), and bacteria (Jin et al., 2004). For several years, the scientific community has been in need of a real-time device for monitoring eATP concentrations to better understand the comprehensive role of this molecule in different physiological processes.

Recently, metal electrodes coated with enzymes have been developed for measuring eATP (Praetorius and Leipziger, 2009). Early biosensor designs were based on amperometric measurements obtained from coupled reactions mediated by the enzymes hexokinase and glucose oxidase. With this approach, ATP changes were correlated to oxidation of the mediator at the sensor surface (i.e. glucose was phosphorylated to glucose 6-phosphate causing a decrease in the electrical signal) (Compagnone and Guilbault, 1997; Kueng et al., 2004). This method was unsuitable for detailed physiological studies not only because of significant sensor interference from the high background glucose present in biological fluids/tissue, but also because the external addition of glucose triggers metabolic activity in the nearby cells, introducing bias on the physiological response of interest.

Work by Llaudet et al. (2005) demonstrated a more specific

* Corresponding author.
E-mail address: emclamor@ufl.edu (E.S. McLamore).

http://dx.doi.org/10.1016/j.bios.2015.05.027
0956-5663/

amperometric detection scheme based on the cascade reactions catalyzed by the enzymes glycerol kinase (GK) and glycerol-3-phosphate oxidase (G3PO). With this approach ATP is measured directly based on glycerol phosphorylation by GK, followed by oxidation of glycerone phosphate to hydrogen peroxide in the second reaction (Murphy and Galley, 1994). Free electrons produced by the deprotonation of peroxide were measured using oxidative amperometry. This micro-biosensor was used to record ATP concentrations near the spinal cord of *Xenopus* embryos during motor activity. The major disadvantage of this device was the interference caused by readily oxidizable molecules such as ascorbate and urate that are commonly present in complex biological samples. In addition, direct measurement of transfer (i.e., flux) was not possible with the static (non-oscillating) microelectrode technique positioned near the *Xenopus* embryo.

Further work by Wang et al. (2013) proposed an optical technique for detecting ATP based on the same cascade reaction catalyzed by GK and G3PO. In this case the enzymes were immobilized onto an optical fiber modified with an oxygen-sensitive dye that responds to oxygen consumption during the oxidation of glycerol-3-phosphate to dihydroxyacetone phosphate. This optical biosensor was successfully applied for monitoring extracellular concentrations of ATP in porcine intervertebral discs. The biosensor did not exhibit any interference in the presence of ascorbate, which is a major advantage over the previous electrochemical-based devices. However, at least two issues need to be considered when using this technique for physiology studies. First, oxygen levels are widely variable in the dynamic environment near living cells and tissues, which requires a compensation method for the biosensor and simultaneous recording of oxygen in the microenvironment near the ATP sensor. Second, reactive oxygen species are produced as a by-product of the working cascade reaction. The enzymatically produced hydrogen peroxide is readily decomposed at ambient conditions, releasing molecular oxygen near the dye which leads to false positive signals since the device is based on measuring oxygen at the sensor surface with an oxygen-quenched luminescent dye.

In general, the high interference caused by naturally occurring molecules in complex samples, the relatively low signal-to-noise ratio (particularly when applied in the cell/tissue domain), and the inability to monitor intricate transport patterns at low analyte concentrations are the foremost limitations of static ATP concentration probes for applications in physiology research. A microsensor modality known as self-referencing (SR) has proven useful for overcoming the most common limitations of static (i.e., non-oscillating) analytical techniques, including: direct non-invasive measurement of flux, high spatial resolution ($\leq$1 μm), significantly increased signal-to-noise ratio and reduced drift/noise (Porterfield, 2007; McLamore and Porterfield, 2011; Vanegas et al., 2013). The SR technique involves oscillation of a microsensor with computer controlled stepper motors, which allows quantification of biophysical transport phenomena at the tissue, cellular and sub-cellular domains (see scheme 1). Over the last few decades, SR sensors have been applied in several physiology studies, targeting analytes such as ions (e.g. Ca^{2+}, H^{+}, K^{+}, and Na^{+}), oxygen, electroactive molecules (e.g. nitric oxide, indole acetic acid), and biomolecules (e.g. glucose, glutamate and lactate) (Mclamore and Porterfield, 2011, 2013; McLamore et al., 2010; McLamore et al., 2010, 2011; Porterfield, 2007; Shi et al., 2011; Gilliham et al., 2006; Land et al., 1999; Sanchez et al., 2008; Zuberi et al., 2008; Dey and Raj, 2010; Borgens, 1984).

We demonstrate for the first time a nanomaterial-mediated SR biosensor for profiling eATP flux in developing fern spores and juvenile plant roots. The bi-enzyme microsensor was fabricated by encapsulating glycerol kinase (GK) and glycerol-3-phosphate oxidase (G3PO) in a laponite sol gel. A stratified bi-enzyme nanocomposite was created on a graphene-functionalized platinum microelectrode using a protein-templated silica nanoshell layer. This protein-templated silica nanoshell layer has proven to effectively encapsulate cells, proteins and other biomacromolecules in gels without significantly limiting diffusion-mediated transport of small molecules in a number of applications Jaroch et al. (2011). The developed biosensor opens the possibility of investigating the underlying mechanisms governing eATP transport in a variety of biological systems. Although we focus on plant tissues in this proof of concept study, the SR ATP microsensor is applicable to any living tissue, with broad applications spanning medical, environmental, and agricultural studies.

2. Experimental

2.1. Materials and Reagents

Adenosine 5′-triphosphate disodium salt hydrate (ATP), chloroplatinic acid 8 wt%, lead acetate 30% w/v, Nafion® 117 solution and MS media were purchased from Sigma-Aldrich (St. Louis, MO). Glycerol kinase (GK), and glycerol-3-phosphate oxidase (G3PO) were purchased from MP Biomedicals (Solon, OH). Glycerol, L-ascorbic acid (AA) was purchased from Fisher Scientific (Pittsburgh, PA), Laponite RD was obtained from Southern Clay Products Inc. (Austin, TX). Tetra-ethyl Orthosilicate (TEOS), potassium nitrate (KNO_3), and hydrochloric acid (37% HCl) were obtained from Acros Organics (New Jersey, NY). Single-layer graphene oxide (GO)

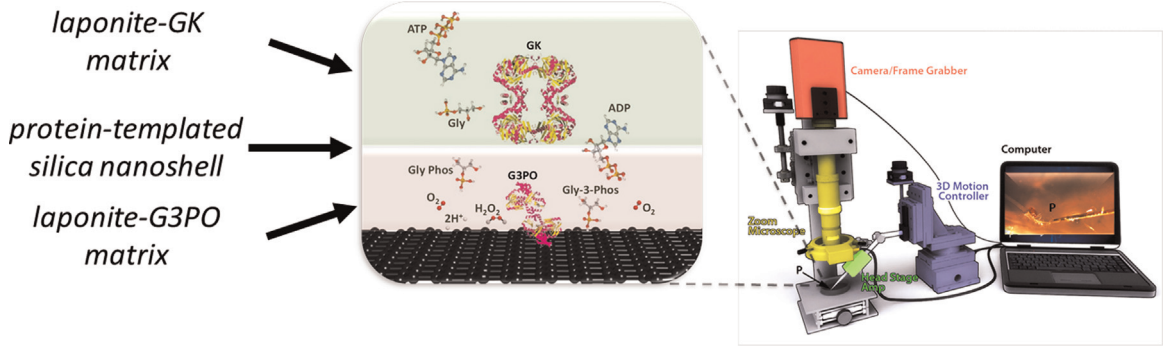

Scheme 1. Schematic of self-referencing micro-biosensor for *in vivo* monitoring of eATP flux in plant systems. The device consists of a camera/zoomscope with framegrabber, 3D motion control system, micro-biosensor (P), and head stage amplifier (main amplifier not shown). Physiological activity is directly measured by recording differential ATP concentration during oscillation of a single micro-biosensor over a fixed excursion distance from the plant surface. Inset depicts the sensing mechanism of the probe which is based on the cascade reaction catalyzed by glycerol kinase (GK) and glycerol-3-phosphate oxidase (G3PO). A stratified bi-enzyme nano-composite was created using a protein-templated silica nanoshell layer. GK and G3PO structure courtesy of protein data bank.

(Thickness: ~0.8 to 1.2 nm; purity: ~99%; manufacturing method: modified Hummer) was procured from ACS Material (Medford, MA). Potassium ferrocyanide trihydrate ($K_3Fe(CN)_6$) was purchased from EMD chemicals (Billerica, MA). PBS and TRIZMA buffers were procured from Mediatech, Inc. (Manassas, VA).

2.2. Biological samples

Corn (*Zea mays* L. cv Merit) seeds were hydrated and soaked overnight in autoclaved water and then placed between wet germination paper in the dark. After 3.5 days the etiolated seedlings were transferred into the light on plates containing MS media in 1% agar. After the transfer they were allowed to recover for 15 minutes before ATP flux measurements were made on root tips.

Ceratopteris richardii (RN5 wt) spores were surface sterilized using 20% bleach, rinsed three times with autoclaved water, and soaked in autoclaved water for 7 days in the dark. After 7 days, water was removed and 10 mL of ½-strength MS, pH 6.3 was added to each 15 mL tube of spores. The tubes were placed in a 28 °C growth chamber for 16 h. Spores were immobilized on 100 μm mesh and allowed to settle for 30 min prior to ATP flux measurements.

2.3. Nanomaterial platform and protein Immobilization

Based on a methodology similar to the one described by Vanegas et al. (2014), a nanocomposite of reduced graphene oxide and nanoplatinum (rGO/nPt) was deposited on the tip of a Pt/Ir microelectrode (PI20033.0A10 MicroProbes©, 1–2 μm tip diameter, Gaithersburg, MD). Briefly, a GO solution was prepared in DI water at a concentration of 2 mg/mL, followed by ultrasonication for 30 min. Next, AA was added to the GO solution at a concentration of 8 mg/mL to partially reduce the graphene oxide sheets (rGO). The tip of the microelectrode was first dip coated with the rGO suspension and allowed to dry at room temperature for 20 min. Next, nanoplatinum clusters were formed on the surface of the electrode via sonoelectrodeposition at 10 V for 30 s in a solution of 0.728% chloroplatinic acid and 0.002% lead acetate (Chaturvedi et al., 2014; McLamore et al., 2011). In order to facilitate charge and size exclusion of potential interfering substances, a Nafion membrane was incorporated on top of the nanomaterial platform by dipping the tip of the microelectrode in Nafion solution for 20 min and then baking the electrode at 115 °C for 1 h.

The stratified bi-enzyme composite (i.e. distinct GK and G3PO layers) was immobilized on the surface of the rGO/nPt-modified microelectrode using a layered encapsulation/entrapment approach with laponite hydrogel and silica sol–gel. Laponite hydrogel (1 wt%) was prepared in TRIZMA buffer and ultrasonicated for 1 h; silica sol–gel solution was prepared by mixing 5 g of TEOS with 4.33 g of deionized water and 2.3 g of HCl (0.04 M) followed by vortex-agitation for 1 h (Jaroch et al., 2011; Jaroch and Rickus, 2011). In order to prepare the bioactive laponite hydrogels, a 10 μL aliquot of laponite (1 wt%) was mixed with 1 mg of either G3PO or GK, and vortex-agitated for 5 min. First, the microelectrode tip was soaked in the laponite–G3PO gel for 1 h followed by dip coating in sol–gel solution for 1 min. Next, the microelectrode tip was soaked in the laponite–GK gel for 1 h followed by dip-coating in sol–gel solution for 1 min.

2.4. Electrochemical characterization

DC potential amperometry (DCPA) was conducted in a working solutions of either TRIZMA buffer or MS media with 1 mM glycerol based on methods described in Vanegas et al. (2014). The biosensor was polarized at constant potential of +700 mV versus Ag/AgCl reference electrode with a sampling rate of 1 kHz; the electrical output signal was recorded while successively injecting ATP into the working solution. Amperometric sensitivity was determined as the slope of the linear portion in the calibration curve. Response time (t_{95}) was determined as the average time required to reach 95% of the steady state response after injecting ATP into the working solution. Lower limit of detection (LOD) was determined as the smallest ATP concentration that can be measured by the sensor based on the 3σ method. Signal-to-noise ratio (S/N) was calculated as the variance ratio between the electrical signal and the background noise.

2.5. Self-referencing amperometry (flux analysis)

Flux measurements were conducted using a SR rig composed of a vibration isolation table with faraday cage (Technical Manufacturing Co. Peabody, MA, USA). Camera/zoomscope (Applicable Electronics, Inc., Sandwich, MA, USA), working and reference electrodes were hooked to a head stage and connected to a motion control system. A/D boards (analogue-to-digital) with DC coupled differential amplifier, and low/high pass filters were used for signal processing/acquisition (Applicable Electronics, Inc., Sandwich, MA, USA). Automated Scanning Electrode Technique software (ASET 2.10) was used for data acquisition. Preamplifier signals were coupled through offset function to discretely subtract off baseline signals (DC coupling) allowing waveform amplification for subsequent digital analysis of differential signals (McLamore and Porterfield, 2011; Porterfield, 2007). Flux measurements from SR amperometry were computed based on Fick's first law of diffusion:

$$J = -D\frac{\Delta C}{\Delta x} = -D\frac{\left(\frac{i_x - i_{x+\Delta x}}{m}\right)}{\Delta x}$$

where: J is the analyte flux, D is the molecular diffusion constant of ATP (2.6×10^{-6} cm^2 s^{-1}), ΔC is the differential analyte concentration, Δx is the fixed excursion distance, i_x is the current measured at the near pole, $i_{x+\Delta x}$ is the current measured at the far pole, and m is the linear slope of the sensor's calibration curve.

To verify use of the ATP under abiotic, controlled, conditions, a step-back experiment was conducted using the methods in McLamore et al. (2011) and McLamore et al. (2009). Briefly, a pulled pipette (1.5 μm diameter, World precision Instruments, Sarasota, FL) was filled with 15 mM ATP dissolved in 2% agarose gel. The gel was solidified at 4 °C for 30 min, and then the pipette was mounted in a three-axis manual micromanipulator (World precision Instruments, Sarasota, FL) with a resolution of 0.1 μm. The micromanipulator was placed in the Faraday cage and immersed in a Petri dish containing 10 mL of TRIZMA buffer with 1 mM glycerol (the same working solution used for the biological experiments). The concentration gradient near the open pipette tip was allowed to stabilize for 30 min. After 30 min, a calibrated ATP microsensor was used to verify that a steady-state ATP concentration gradient was established in the solution near the pipette tip (see Supplemental Fig. S1). For conducting the step-back experiment, the micro-biosensor was positioned at the surface of the pipette tip (within 1 μm) and oscillated at an oscillation frequency of 0.33 Hz perpendicular to the tangent of the tip surface (Δx=30 μm). After recording a minimum of nine measurements, the sensor was positioned 5 μm away from the pipette tip and flux measurements were recorded again. This step-back protocol was repeated until there was no significant change (< 1%) in ATP flux. A Fickian transport model (McLamore et al., 2009) was used for predicting the expected flux profile in the bath solution based on the concentration gradient (Δx), excursion distance (Δx), temperature, and diffusion constant (D). The correlation coefficient between measured and predicted flux was calculated to

characterize goodness of fit (Mclamore and Porterfield, 2011, 2013; McLamore et al., 2011; Porterfield, 2007).

2.6. ATP flux in plant roots

Corn seedlings were grown in the dark for 3.5 days and then carefully transferred to an MS agar plate. Prior to measurements the plates were angled at 45 degrees and the roots were equilibrated with MS solution for several minutes. Roots were wounded in the distal elongation zone (approximately 1000 μm from the root tip) using 3 mm (100 μm tip point) stainless steel McPherson-Vannas Scissors (World Precision Instruments, Sarasota, FL). Sensor measurements were taken prior to wounding to determine unwounded levels and then immediately after wounding or touching for 30 min.

2.7. ATP flux measurement in fern spores

Ceratopteris spores were grown at 28 °C for 16 h before being immobilized on 100 μm nylon mesh that was fixed and submerged in ½-strength MS, pH 6.3. The spores were allowed to settle for 30 min prior to ATP flux measurements. Measurements were taken on the surface of germinating spores for 30 min per spore location.

2.8. Imaging

To image carbon and platinum nanomaterials, scanning electron microscopy (SEM) micrographs were taken using a JEOL 5600 LV, with accelerating voltage of 20–30 kV as described in Vanegas et al. (2014). In order to corroborate the presence and distribution of GK and G3PO in the hydrogel/sol–gel matrix, laser scanning confocal microscopy (LSCM) images were taken using an Olympus FV1000 (Shinjuku, Japan) 6 laser multiscanning confocal system mounted on an Olympus IX81 inverted microscope. GK was directly labelled with Dylight 488 (Thermo Scientific, green; $\lambda = 493/518$ nm); G3PO was labelled with Dylight 594 (Thermo Scientific, red; $\lambda = 594/613$ nm). Image capture and processing was performed with Olympus Fluoview Version 3.1b software.

2.9. Statistics

For statistical inference, all measurements were made at least in triplicate as independent experiments based on a completely randomized design. Differences between variables were tested for significance by analysis of variance (ANOVA, model I). Significantly different means ($P < 0.05$, $\alpha = 0.05$) were separated by Tukey tests (error rate = 0.05). Minitab® 15 (Minitab Inc., State College, Pennsylvania) was used for statistical analyses. Graphs were made using SigmaPlot 12.5 (Systat Software Inc., San Jose, California).

3. Results and discussion

3.1. Biosensor fabrication and performance characterization

The surface features of the rGO/nPt platform are shown in the left panel of Fig. 1. Previous work by Vanegas et al. (2014) demonstrated the capability of this hybrid nanomaterial to enhance the electrochemical performance of amperometric sensors by vastly increasing the contact interface, as well as potentiating the electrical behaviour of the transducing component. The relatively high electroactive area of the rGO/nPt platform also permits larger enzymatic loading onto the sensor surface (compared to other nanomaterial platforms such as carbon nanotubes; see Vanegas et al. (2014) for detailed discussion). Distribution of the enzymes within the hydrogel/sol–gel matrix was characterized by LSCM to emphasize the presence and distribution of each type of enzyme (right panel of Fig. 1). Preliminary fundamental electrochemical studies (data not included) indicated sensors based on GK and G3PO mixed into the same gel had a low reproducibility. For that reason, a scaffold format was used to create distinct stratified zones of GK and G3PO separated by a protein-templated silica nanoshell. Laponite hydrogel was selected as a protein encapsulant due to the high charge-exchange capacity (Macha and Fitch, 1998; Xiang and Villemure, 1995; Neumann and Sansom, 1970). Silica sol–gel was utilized to form a protein-templated nanoshell layer between the two layers of bioactive hydrogels based on our previous work (Jaroch et al., 2011). Jaroch et al. (2011) showed that these protein-templated silica layers form a 100 nm thick layer with pore sizes of approximately 10 nm, preventing enzyme detachment while allowing movement of molecules (e.g. ATP, glycerol, O_2, etc.) between the hydrogel layers. As discussed by Jaroch et al. (2011) in detail, the proteins serve as a template for the preferential nucleation of silica to form the nanoshell in aqueous solution at near-neutral (pH 6–8), which is a major advantage over other silica sol gel protocols which require gelation at non-neutral pH.

Standard electrochemical experiments were conducted to determine the performance characteristics of the ATP micro-

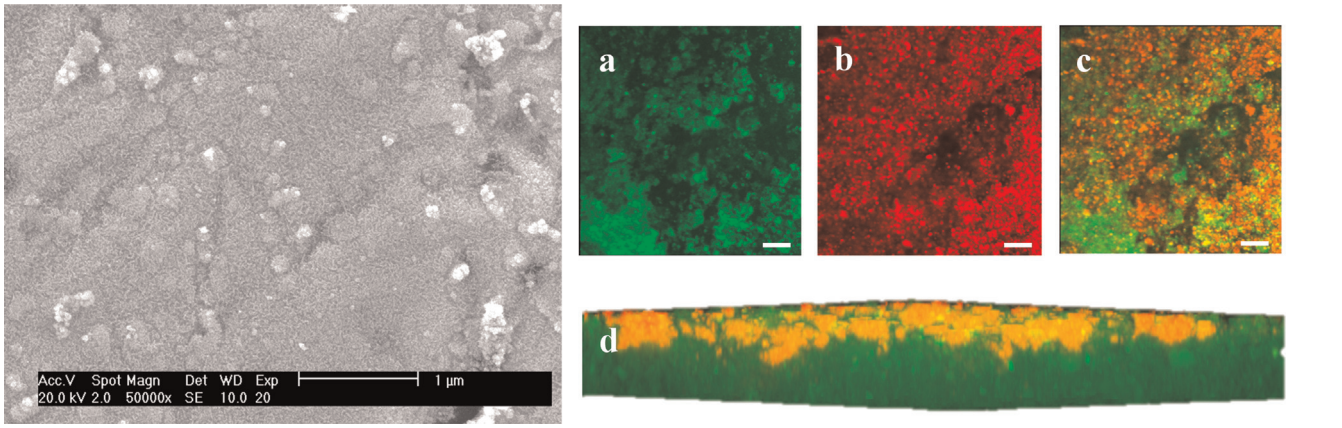

Fig. 1. Sensor functionalization with electrocatalytic nanomaterials and bioactive hydrogels. Left panel: SEM micrograph of rGO/nPt platform showing surface features of the nanomaterial-modified electrode. Right panel: LSCM images of hydrogel/bi-enzyme matrix. (a) GK directly labelled with Dylight 488 (Thermo Scientific, green) showing the enzyme distribution in the first hydrogel layer. (b) G3PO directly labelled with Dylight 594 (Thermo Scientific, red) depicting the enzyme distribution in the second hydrogel layer. (c) overlaid image of (a) and (b) showing the co-localization of the two enzymes in the matrix. (d) z-map displaying a distinct separation between the two layers of bioactive hydrogel. Scale bars: 10 μm.

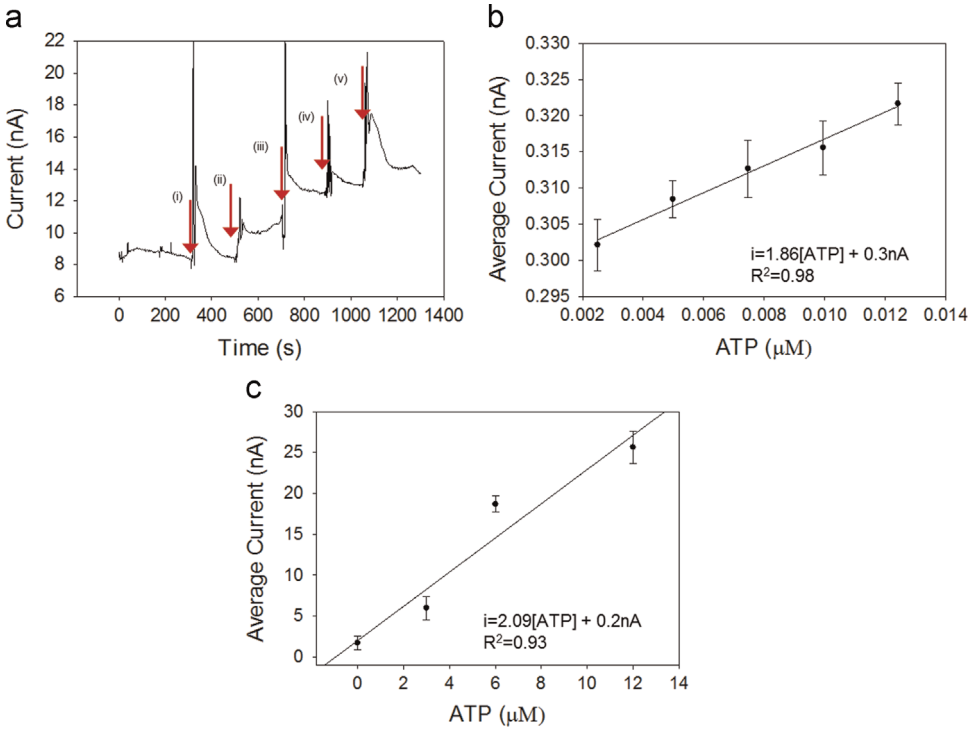

Fig. 2. Electrochemical performance of ATP micro-biosensor. (a) Representative DCPA curve showing the change in current output after injecting ATP into the working solution (arrows indicate the injection times: (i) 3 μM, (ii) 6 μM, (iii) 9 μM, (iv) 15 μM and (v) 21 μM). (b) Representative calibration curve showing the steady state response of the biosensor to increasing analyte in the low-concentration range. (c) Representative calibration curve showing the steady state response of the biosensor to increasing analyte in the high-concentration range. The sensitivity of the probe was calculated as the slope of the linear portion in the calibration curves.

biosensor. Fig. 2a shows a representative real-time DCPA curve in which the current signal shifts rapidly after each addition of ATP into the working solution. The steady state values of the electrical response were correlated with the concentration of ATP in the electrochemical cell to generate the average calibration plots (see Fig. 2b and c for representative plots of calibration at low and high ATP concentration, respectively). Based on these data, the micro-biosensor exhibited a sensitivity of 2.4 ± 1.8 nA/μM, a response time of 20 ± 13 s, a lower detection limit of 1.3 ± 0.7 nM, and a $S/N \geq 3$. In a seven day study, the biosensor sensitivity did not decrease significantly ($1.33 \pm 0.52\%$ decrease in sensitivity). These performance characteristics are similar and in some cases superior to the previously reported biosensor devices (see Table 1 for details). Furthermore, inclusion of a Nafion membrane on the transducing platform significantly diminished the effect of interferent compounds (see Supplemental Fig. S2) improving the selectivity of the probe and allowing for a higher signal-to-noise ratio.

The operating range of the ATP microsensor in this study (1.3–12 μM) spans the expected range of ATP in biological fluids from animals, bacteria and plants based on results obtained using the luciferase assay (see Supplemental Fig. S3). According to Gorman et al. (2007), human plasma ATP concentrations range from 1 μM in healthy individuals to as low as 28 nM. Silva-Ramos et al. (2013) recorded levels of urinary ATP in the range of 2–6 nM for healthy patients and 7–11 nM for patients with overactive bladder syndrome. Jin et al. (2004) found ATP concentrations ranging from 2.5 to 32 nM in oral *Candida albicans* biofilms. Lim et al. (2014)

Table 1
Summary of biosensors for measuring eATP in physiological research.

Approach	Biorecognition Scheme	Sensitivity [t_{95}]	LOD	Application	Reference
Optical	GK/G3PO immobilized on an optical fiber	−104 mM μs [0.1 ms]	1 μM	Porcine intervertebral disc	Wang et al. (2013)
DVP, EIS	DNA aptamer immobilized on gold electrode	NR	20 fM	Human serum	Liu et al. (2014)
Amp	HEX/GOx immobilized on a Pt electrode.	≈ 2 nA mM^{-1} [≈ 2–3 min]	0.01 mM	Human erythrocyte hemolysate	Compagnone and Guilbault (1997)
Amp	HEX/GOx immobilized on a Pt electrode.	≈ 3 μA mM^{-1} [5 s]	10 nM	NR	Kueng et al. (2004)
Amp	GK/G3PO sol gel immobilized on microelectrode	≈ 0.3 μA mM^{-1} [< 10 s]	200 nM	Spinal cord of *Xenopus* embryos	Llaudet, et al. (2005)
Amp	Stratified GK/G3PO nano-composite on microelectrode	2.4 ± 1.8 nA μM^{-1} [20 ± 13 s]	1.3 ± 0.7 nM	*Ceratopteris* spores and *Zea mays* roots	This work

DVP=differential pulse voltammetry;
EIS=electrochemical impedance spectroscopy;
Amp=amperometry;
GK=glycerol kinase;
G3PO=glycerol 3 phosphate oxidase;
HEX=hexokinase;
GOx=glucose oxidase;
NR= not reported

found eATP levels in the 2–4 nM range near healthy *Arabidopsis thaliana* roots, and Song et al. (2006) measured ATP as high as 40 μM in wounded *A. thaliana* roots. The micro-biosensor is directly applicable to each of these studies, although the most unique aspect of the technique is the direct measurement of flux near the cell/tissue surface (see Fig. 4 and related discussion).

Importantly, the limit of detection for the stratified bi-enzyme sensor developed here was significantly lower than nearly all previous devices that directly measure ATP in a reversible manner. The device by Kueng et al. (2004) reported a limit of detection that was lower (10 nM), but the device was based on glucose oxidase activity and did not directly measure ATP. Liu et al. (2014) report the lowest LOD in the literature (20 fM), however the device is based on hysteric binding between ATP and a protein-binding nucleotide sequence (a type of aptamer known as a concatamer). Liu et al. (2014) demonstrated ATP specific binding using differential pulse voltammetry in the presence of ATP analogues (guanosine triphosphate, cytidine triphosphate, uridine triphosphate, and thymidine triphosphate). The problem with this device for real time measurements of ATP release kinetics is that the concatamer is designed to irreversibly bind ATP to produce a change in charge transfer resistance or faradaic current. Thus, the device cannot be used to produce quantitative flux data in experiments where the ATP concentrations are changing rapidly (and transient flux is spatially reversible). Although the sensitivity and response time for our microsensor are not significantly improved over some previous electrochemical devices (such as the device by Llaudet et al. (2005)), to date there have been no demonstrations of a SR flux sensor used to measure the direction and magnitude of ATP flux near living cells. This is an important contribution, since ATP is an active signaling molecule in the extracellular environment near living cells. Other studies have documented the active release of ATP by animal and plant cells, the hydrolysis of ATP to ADP and of ADP to AMP by an extracellular enzyme known as apyrase (Clark et al., 2011, 2014), and also the activation of purinoceptors by extracellular nucleotides (Fitz, 2007). These studies are discussed in Clark et al. (2014) and others in the eATP signaling field suggesting that ATP transport outside the cell is highly dynamic. To validate the use of the SR eATP microsensor for such biological applications, a series of abiotic and biological validation studies were performed.

3.2. Abiotic validation of ATP flux

Following calibration, abiotic validation of ATP flux was achieved by measuring the concentration gradient within the diffusion layer formed by a point source of ATP (made of 15 mM ATP and 2% agar) suspended in an unestirred solution of PBS with 0.1% glycerol. The oscillation frequency was maintained at 0.33 Hz, since previous literature indicated that sensors operating below 0.20 Hz are subjected to wide background noise and underestimation of anlyte levels (McLamore and Porterfield, 2011; McLamore et al., 2010a; Shi et al., 2011; Kuhtreiber and Jaffe, 1990). An empirical Fickian model was aslo included based on McLamore et al. (2009), see Supplemental Fig. S1 for concentration profile used to develop the model. The correlation (ε) between the measured flux data and the model prediction for abiotic flux experiments was 0.98 (Fig. 3), thus ratifying the application of Fick's first law of diffusion and validating the use of the ATP microbiosensor in the SR modality.

3.3. Physiological eATP flux in spores and roots

One of the most obvious situations in which cells would be expected to release ATP is during wounding, which would allow cytoplasmic ATP that is in the mM range (Gout et al., 1992) to flow out into the extracellular matrix near cells. Previous luciferin–luciferase assays of fluid collected from wound sites of *Arabidopsis* leaves found that these bulk samples accumulated an average of 40 μM ATP (Song et al., 2006). Touch stimulation also induces the release of ATP from plant cells (Jeter et al., 2004; Weerasinghe et al., 2009). Thus, as a first test of our novel biosensor we chose to measure the eATP released from corn roots in response to wounding and touching (see Supplemental Figure S4 for photographs during the experiment). Prior to wound or touch stimulation the concentration of eATP outside of corn root tips was determined to be 2.6 ± 0.3 nM using the micro-biosensor (Fig. 4a). This measurement of [eATP] corresponds well to recent measurements of low nanomolar concentrations of ATP (2–5 nM) in the media of growing *Arabidopsis* roots (Lim et al., 2014). After the corn roots were wounded, the micro-biosensor detected an increase in the [eATP] to 3.4 ± 0.1 μM. This [eATP] is about 10-fold lower than the average value obtained from leaf sap measurements obtained by Song et al. (2006) after leaves were wounded. The higher [eATP] in the leaf sap could be expected in that actively photosynthesizing leaf cells are likely to have higher cytoplasmic [ATP] than root cells, and that apyrase enzymes that hydrolyze ATP are poorly expressed in mature leaves, but are expressed highly in growing roots (Wu et al., 2007). Touching corn roots (using a 1 mm wire and computer controlled stepper motors) induced approximately a 4-fold increase in the [eATP] to 10.4 ± 2.9 nM as detected by the micro-biosensor. This result is in accordance with the expectation that the touch stimulus would induce a substantially lower increase in the level of eATP than wounding would. Based on the results from ANOVA and Tukey tests, we found sufficient evidence ($p < 0.05$) that both concentration and

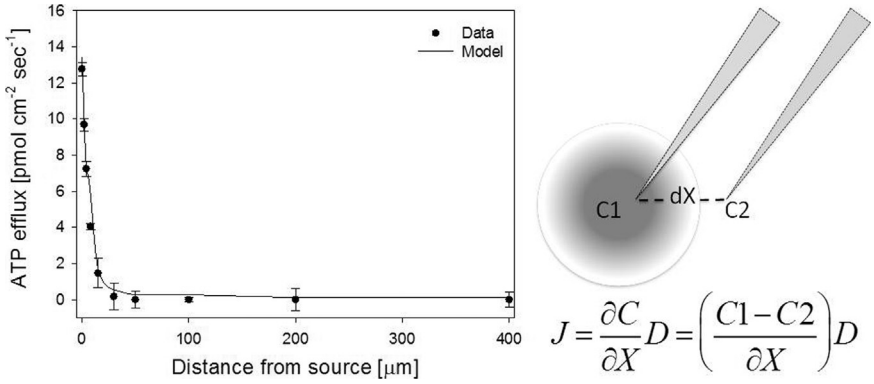

Fig. 3. Abiotic validation of SR ATP micro-biosensor. Validation was achieved by measuring the gradient formed near the tip of a pulled micropipette filled with 15 mM ATP and 2% agar immersed in PBS with 0.1% glycerol. Dots and error bars indicate mean and standard deviation of the measured data ($n=3$) and solid line indicates predicted value based on empirical Fickian diffusion model ($\varepsilon=0.98$).

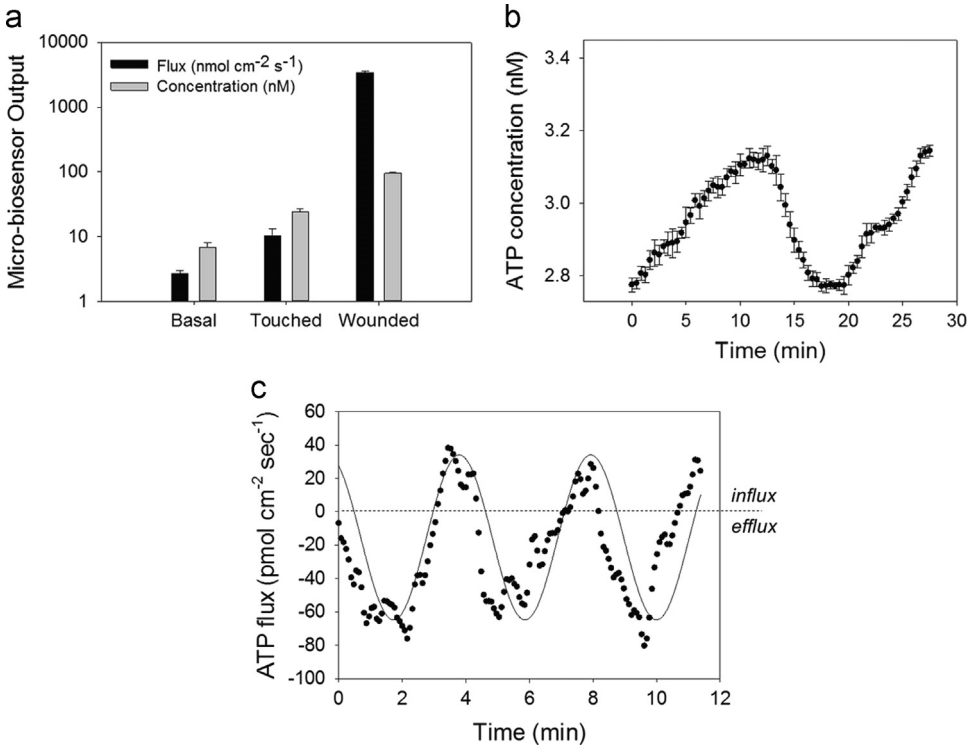

Fig. 4. (a) Mechanical stimulation and wounding experiment in *Zea mays* roots. Grey bars show the ATP concentration, and black bars show the ATP flux. The roots were immersed in PBS buffer with 0.1% glycerol; the probe was positioned at about 50 μm from the tip of the root to monitor eATP before mechanical stimulation (noted as "basal"), after mechanical stimulation (by touching the root with a 1 mm platinum wire), and after wounding the root with microsurgical tweezers. The mean concentration and efflux near the surface of the basal/untouched (2.6 nM and 6.9 nmol cm^{-2} s^{-1} respectively), touched (10.4 nM and 24.0 nmol cm^{-2} s^{-1} respectively) and wounded root (3.4 μM and 95.0 nmol cm^{-2} s^{-1} respectively) were significantly different ($p < 0.01$); error bars indicate the standard deviation from the mean ($n=6$). (b) Average ATP concentration recorded near the surface of developing *Ceratopteris* spores immobilized in 100 μm Nylon mesh ($n=12$). (c) Representative real-time measurement of ATP flux at the surface of a spore within the first hour of light exposure.

efflux are significantly different among baseline, touched, and wounded roots.

Ceratopteris fern spores are another model system for studying the role of ATP release in plant growth and development. In these spores, gravity-directed polarization is fixed during the first 24 h of development. In order to determine if eATP plays a role in this physiological process, spores were exposed to a poorly-hydrolysable form of ATP, ATPγS, and an antagonist of extracellular nucleotide receptors, pyridoxal phosphate-6-azo(benzene-2,4-disulfonic acid) tetrasodium salt hydrate (PPADS) for the first 24 h of development. As a result of these treatments, *Ceratopteris* spores had a statistically significant decrease in the number of downward growing rhizoids, a visual representation of the direction of polarization set by environmental cues, largely gravity (Bushart et al., 2013). The micro-biosensor was used to confirm the release of ATP during the initiation of spore polarization (see Supplemental Fig. S5 for schematic and photographs of the experimetnal set up). Fig. 4b shows the average time series for concentration data recorded at the surface of the spores. Within the first 30 min of light exposure, the concentration of eATP near the surface of the spore reached a maximum of 5.0–6.5 nM. The concentration near the surface was temporally dynamic; there was a wave of ATP released in cycles of approximately 10–12 minutes, followed by a decrease in surface concentration that lasted approximately 6–9 min; the minimum ATP concentration during this bursting behaviour was 1.5–3.0 nM. The flux measurements at the spore surface showed that during this transient ATP release results in a net efflux of ATP during spore polarization (Fig. 4c; negative values are shown as efflux and positive values are shown as influx). The average net efflux was 13.2 ± 4.8 pmol-ATP h^{-1}. To calculate the release rate, an emprical harmonic oscillator model was developed based on the methods developed by McLamore et al. (2010b). The parameters for the simple harmonic oscillator are shown in the supplemental section (Supplemetnal Eq. E1). These results support the hypothesis that ATP is released during early growth and development of *Ceratopteris* spores, although more experiments are needed to determine the dynamics of ATP release, apyrase activity, and receptor-mediated uptake.

To date, assays of extracellular ATP outside of plant cells have all depended on the use of luciferin/luciferase-based methods. These methods accurately quantify [eATP] as it is diluted into media around cells, but thus far they have yielded only relative measurements in regions immediately near the extracellular matrix of intact living cells (Kim et al., 2006; Clark et al., 2010). In contrast, the micro-biosensor approach described here can be used to quantify the [eATP] in the immediate vicinity of any intact plant cell or tissue.

4. Conclusions

We developed an electrochemical micro-biosensor for monitoring the dynamics of eATP in plant cells/tissue. The working principle was based on the coupled biochemical reaction catalyzed by the enzymes GK and G3PO. The micro-biosensor utilized a hybrid transducing component made of rGO, nPt and Nafion, which greatly enhances the sensitivity, response time, limit of detection, and selectivity of the device. The micro-biosensor was demonstrated in the self-referencing mode for studying transmembrane flux of ATP by corn roots and fern spores. After a series of mechanical stimulation experiments, it was found that eATP levels by wounded roots were significantly higher than those

measured in unwounded tissue. In the case of Ceratopteris spores, the device was used to confirm the release of ATP during the initiation of spore polarization. Our results show the ability of the SR micro-biosensor for monitoring concentration and biophysical transport of eATP, providing a unique tool for testing hypothesis in plant physiology studies. In future detailed studies, the SR ATP sensor will be a powerful tool for monitoring the extracellular transport of ATP under physiological and pathophysiological conditions. Although these proof of concept experiments focus on plant tissues, the technique developed herein is applicable to any living tissue, where nanomolar concentrations of ATP play a critical role in signaling and development.

Acknowledgements

The authors would like to thank the Colombian funding agencies Colfuturo y Colciencias (No. 001375882), the Agricultural and Biological Engineering Department of the University of Florida, and the UF Early Career Award (USDA/NIFA Hatch Project No. FLA-ABE-005062) for the financial support. This study was also supported by NASA grant NAG10-295 to S.J.R. and G.C. The authors also thank Dr. Zhaohui Tong at the University of Florida for donating the laponite hydrogel, and EnCor Biotechnology Inc. (Gainesville, FL) for their assistance with the confocal imaging.

Appendix A. Supplementary information

Supplementary data associated with this article can be found in the online version at http://dx.doi.org/10.1016/j.bios.2015.05.027.

References

Borgens, R.B., 1984. Science 225, 478–482.
Burnstock, G., 2012. Bioessays 34, 218–225.
Bushart, T.J., Cannon, A.E., ul Haque, A., Miguel, San, Mostajeran, P., Clark, K., Porterfield, G.B., Roux, D.M., S.J., 2013. Am. J. Bot. 100, 161–174.
Chaturvedi, P., Vanegas, D.C., Taguchi, M., Burrs, S.L., Sharma, P., McLamore, E.S., 2014. Biosens. Bioelectron. 58, 179–185.
Clark, G., Fraley, D., Steinebrunner, I., Cervantes, A., Onyirimba, J., Liu, A., Torres, J., Tang, W., Kim, J., Roux, S.J., 2011. Plant Physiol. 156, 1740–1753.
Clark, G., Torres, J., Finlayson, S., Guan, X.Y., Handley, C., Lee, J., Kays, J.E., Chen, Z.J., Roux, S.J., 2010. Plant Physiol. 152, 1073–1083.
Clark, G.B., Morgan, R.O., Fernandez, M.P., Salmi, M.L., Roux, S.J., 2014. Plant Sci. 225, 107–116.
Compagnone, D., Guilbault, G.G., 1997. Anal. Chim. Acta 340, 109–113.
Dey, R.S., Raj, C.R., 2010. J. Phys. Chem. C, 21427–21433.
Fitz, J.G., 2007. Trans. Am. Clin. Climatol. Assoc. 118, 199–208.
Gilliham, M., Sullivan, W., Tester, M., Tyerman, S.D., 2006. Plant J. 46, 134–144.
Gorman, M.W., Feigl, E.O., Buffington, C.W., 2007. Clin. Chem. 53 (2), 318–325.
Gout, E., Bligny, R., Douce, R., 1992. Carbon-13 and phosphorus-31 nuclear magnetic resonance studies. J. Biol. Chem. 267, 13903–13909.
Jaroch, D., McLamore, E., Zhang, W., Shi, J., Garland, J., Banks, M.K., Porterfield, D.M., Rickus, J.L., 2011. Biotechnol. Bioeng. 108, 2249–2260.
Jaroch, D.B., Rickus, J.L., 2011. PCT/US2010/042672.
Jeter, C.R., Tang, W.Q., Henaff, E., Butterfield, T., Roux, S.J., 2004. Plant Cell 16, 2652–2664.
Jin, Y., Samaranayake, L.P., Samaranayake, Y., Yip, H.K., 2004. Arch. Oral Biol. 49, 789–798.
Kim, S.-Y., Sivaguru, M., Stacey, G., 2006. Plant Physiol. 142, 984–992.
Kueng, A., Kranz, C., Mizaikoff, B., 2004. Biosens. Bioelectron. 19, 1301–1307.
Kuhtreiber, W.M., Jaffe, L.F., 1990. J Cell Biol 110 (5), 1565–1573.
Land, S.C., Porterfield, D.M., Sanger, R.H., Smith, P.J., 1999. J. Exp. Biol. 202, 211–218.
Lim, M.H., Wu, J., Yao, J., Gallardo, I.F., Dugger, J.W., Webb, L.J., Huang, J., Salmi, M.L., Song, J., Clark, G., Roux, S.J., 2014. Plant Physiol. 164, 2054–2067.
Liu, Z., Chen, S., Liu, B., Wu, J., Zhou, Y., He, L., Ding, J., Liu, J., 2014. Anal. Chem. 86 (24), 12229–12235.
Llaudet, E., Hatz, S., Droniou, M., Dale, N., 2005. Anal. Chem. 77, 3267–3273.
Macha, S.M., Fitch, A., 1998. Mikrochim. Acta 128, 1–18.
McLamore, E.S., Porterfield, D.M., Banks, M.K., 2009. Biotechnol. Bioeng. 102, 791–799.
McLamore, E.S., Diggs, A., Calvo Marzal, P., Shi, J., Blakeslee, J.J., Peer, W., Murphy, A.S., Porterfield, D.M., 2010b. Plant J. 63, 1004–1016.
McLamore, E.S., Mohanty, S., Shi, J., Claussen, J., Jedlicka, S.S., Rickus, J.L., Porterfield, D.M., 2010a. J. Neurosci. Methods 189, 14–22.
McLamore, E.S., Porterfield, D.M., 2011. Chem. Soc. Rev. 40, 5308–5320.
Mclamore, E.S., Porterfield, D.M., 2013. Noninvasive tools for measuring metabolism and biophysical analyte transport at the root-rhizosphere interface: self-referencing electrochemical and optical sensors. In: Eshel, A., Beeckman, T. (Eds.), Plant Roots: The Hidden Half. Taylor & Francis Group,, Boca Raton, FL, pp. 1–18.
McLamore, E.S., Shi, J., Jaroch, D., Claussen, J.C., Uchida, a, Jiang, Y., Zhang, W., Donkin, S.S., Banks, M.K., Buhman, K.K., Teegarden, D., Rickus, J.L., Porterfield, D. M., 2011. Biosens. Bioelectron. 26, 2237–2245.
Murphy, L.J., Galley, P.T., 1994. Anal. Chem. 66 (23), 4345–4353.
Neumann, B., Sansom, K.G., 1970. J. Soc. Cosmet. Chem. 21, 237–258.
Porterfield, D.M., 2007. Biosens. Bioelectron. 22, 1186–1196.
Praetorius, H.A., Leipziger, J., 2009. Purinergic Signal. 5, 433–446.
Sanchez, B.C., Ochoa-AcuÑa, H., Porterfield, D.M., Sepúlveda, M.S., 2008. Environ. Sci. Technol. 42, 7010–7017.
Shi, J., McLamore, E.S., Jaroch, D., Claussen, J.C., Mirmira, R.G., Rickus, J.L., Porterfield, D.M., 2011. Anal. Biochem. 411, 185–193.
Silva-Ramos, M., Silva, I., Oliveira, O., Ferreira, S., Reis, M.J., Oliveira, J.C., Correia-de-Sa´, P., 2013. PLoS One 8 (5), e64696.
Song, C.J., Steinebrunner, I., Wang, X., Stout, S.C., Roux, S.J., 2006. Plant Physiol. 140, 1222–1232.
Vanegas, D.C., Taguchi, M., Chaturvedi, P., Burrs, S., Tan, M., Yamaguchi, H., McLamore, E.S., 2014. Analyst 139, 660–667.
Vanegas, D.C., Taguchi, M., Chaturvedi, P., Burrs, S., 2013. McLamore, E.S.. Smart Biomedical and Physiological Sensor Technology X, 87190N doi:10.1117/12.2016233.
Wang, C., Huang, C.-Y.C., Lin, W.-C., 2013. Biosens. Bioelectron. 43, 355–361.
Weerasinghe, R.R., Swanson, S.J., Okada, S.F., Garrett, M.B., Kim, S.Y., Stacey, G., Boucher, R.C., Gilroy, S., Jones, A.M., 2009. FEBS Lett. 583, 2521–2526.
Wu, J., Steinebrunner, I., Sun, Y., Butterfield, T., Torres, J., Arnold, D., Gonzalez, A., Jacob, F., Reichler, S., Roux, SJ., 2007. Plant Physiol. 144, 961–975.
Xiang, Y., Villemure, G., 1995. J. Electroanal. Chem. 381, 21–27.
Zhang, Y., Phillips, G.J., Li, Q., Yeung, E.S., 2008. Anal. Chem. 80, 9316–9325.
Zuberi, M., Liu-Snyder, P., Ul Haque, A., Porterfield, D.M., Borgens, R.B., 2008. J. Biol. Eng. 2, 17.